RSC Advances

PAPER

View Article Online
View Journal | View Issue

Check for updates

Cite this: *RSC Adv.*, 2021, **11**, 22929

Preparation and characterization of nanofibrous cellulose as solid polymer electrolyte for lithium-ion battery applications

Qolby Sabrina, *[ab] Christin Rina Ratri,[a] Andri Hardiansyah,[a] Titik Lestariningsih,[a] Achmad Subhan,[a] Abdulloh Rifai,[a] Rike Yudianti *[a] and Hiroshi Uyama *[b]

A novel bacterial cellulose (BC)-based nanofiber material has been utilized as an ionic template for the battery system solid polymer electrolyte (SPE). The effect of drying techniques such as oven and freeze-drying on the gel-like material indicate differences in both visual and porous structures. The morphological structure of BC after oven and freeze-drying observed by field-emission scanning electron microscopy indicates that a more compact porous structure is found in freeze-dried BC than oven-dried BC. After the BC-based nanofiber immersion process into lithium hexafluorophosphate solution (1.0 M), the porous structure becomes a host for Li-ions, demonstrated by significant interactions between Li-ions from the salt and the C=O groups of freeze-dried BC as shown in the infrared spectra. X-ray diffraction analysis of freeze-dried BC after immersion in electrolyte solution shows a lower degree of crystallinity, thus allowing an increase in Li-ion movement. As a result, freeze-dried BC has a better ionic conductivity of 2.71×10^{-2} S cm^{-1} than oven-dried BC, 6.00×10^{-3} S cm^{-1}. Freeze-dried BC as SPE also shows a larger electrochemical stability window around 3.5 V, reversible oxidation/reduction peaks at 3.29/3.64 V, and an initial capacity of 18 mAHr g^{-1} at 0.2C. The high tensile strength of the freeze-dried BC membrane of 334 MPa with thermal stability up to 250 °C indicates the potential usage of freeze-dried BC as flexible SPE to dampen ionic leakage transfer.

Received 4th May 2021
Accepted 15th June 2021

DOI: 10.1039/d1ra03480d

rsc.li/rsc-advances

Open Access Article. Published on 29 June 2021. Downloaded on 12/9/2025 8:32:49 AM.
This article is licensed under a Creative Commons Attribution-NonCommercial 3.0 Unported Licence.

Introduction

Lithium-ion batteries (LiBs) have been widely used in portable electronics and developed as power sources in electric vehicles and stationary energy storage in renewable energies. With the rapid development of LIBs for high power applications, safety becomes a significant concern for batteries due to flammable organic liquid electrolytes. Solid polymer electrolyte (SPE) is considered to tackle the safety issue. Due to the non-flammable properties of solid electrolytes, LiBs are expected to exhibit fewer side reactions and higher safety. The use of SPE promises solutions to the leakage, evaporation, and degradation of LiBs containing liquid electrolytes that are still widely used today. SPE also helps to improve dendrite puncture resistance during the recharge process, which enhance its shelf life. SPE could promote dendrite-free stable lithium deposition which opens up new possibilities for research.[1,2]

SPE plays a critical role in facilitating ion transport and functions as the separation membrane between the cathode and the anode in the battery system.[3] Batteries with SPE provide a long charge–discharge life cycle. However, SPE has a small current density because of low ionic conductivity compared with aqueous-based electrolyte. In recent years, several polymeric materials as electrolyte matrices have been developed.[4] Poly(ethylene oxide) (PEO) produced commercially has been used as an electrolyte membrane. A good SPE requires high ionic conductivity, low toxicity, good mechanical properties, and high thermal stability. In PEO, at high temperatures, its ionic conductivity tends to decrease due to reducing membrane moisture.[5,6] In addition, PEO has poor mechanical properties resulting in easy ion leakage, where as the flexible polymer electrolyte is advantageous for good contact between electrode and electrolyte. Currently, SPE research focuses on providing the right environment for the dissolution of lithium salts and suitable cations because the interaction between lithium ions and electron donors of the polymer chains leads to low ionic mobility. The formation of pores across the membrane may facilitate the process of lithium-ion intercalation on LiB.[7] Ion transport will be easier on the polymer nanoporous structure.

Bacterial cellulose (BC) is an environmentally friendly material that possesses a nanofibrous cellulosic structure. Strong intermolecular hydrogen bonds provide superior mechanical performance, thermal stability, and dielectric properties.[8] The nanofibrous structure of BC also has excellent porosity, flexibility

[a]*Research Center for Physics, Indonesian Institute of Sciences, Kawasan Puspiptek Serpong Gd. 442 Tangerang Selatan, Banten 15314, Indonesia. E-mail: qolby89@gmail.com; qolb001@lipi.go.id*

[b]*Department of Applied Chemistry, Graduate School of Engineering, Osaka University, 2-1 Yamadaoka, Suita, Osaka 565-0871, Japan*

© 2021 The Author(s). Published by the Royal Society of Chemistry

Open Access Article. Published on 29 June 2021. Downloaded on 12/9/2025 8:32:49 AM.
This article is licensed under a Creative Commons Attribution-NonCommercial 3.0 Unported Licence.

in surface functionalities, and heteroatoms (oxygen atoms) with free pair of electrons which facilitate ionic conduction. The layered BC with the compact porous structure in the composite provides efficiency for the wetting of the electrolyte and the uniformity of the ion flux, so that guarantee the electrolyte absorbent capacity and provide abundant ionic passageways.[9,10]

In recent work, we reported the utilization of BC as SPE of LiB. BC is preferred to be used as a flexible membrane and endows Li^+ transport between electrodes. BC-based nanofibers materials were prepared with two dry treatments to allow cross-linking reactions to take place. Two drying techniques, such as oven and freeze-drying, were subjected to BC to develop its dissociation, adsorption, retaining, and accelerating the migration of lithium ions from the electrolyte solution added to BC. Several material characterizations were performed to examine the potential application of the BC as SPE in LiB. Structure and mechanical properties were investigated by using field-emission scanning electron microscopy (FESEM), Fourier-transform infrared (FTIR) spectroscopy, X-ray diffraction (XRD), thermo gravimetric analysis (TGA), tensile test, and Brunauer–Emmet–Teller (BET) analysis. Electrochemical performances were examined by using electrochemical impedance spectroscopy (EIS), linear sweep, cyclic voltammetry, and charge–discharge (CD) measurements.

Experimental

Preparation of oven- and freeze-dried BC

BC gel was purchased from small enterprise coconut local farmers. BCs with an area size of 3 × 3 cm^2 underwent a neutralization process by boiling the BCs in deionized water for 1 h. Subsequently, the samples were soaked in ethanol for two days to improve the porous structure, including pore size and morphology.[11,12] Two sets of samples were prepared, including oven- and freeze-dried BC. For the oven-dried BCs, the samples were oven-dried in 60 °C for one day. Freeze-drying treatment of the samples for freeze-dried BCs was conducted using a freeze dryer (BUCHI L-300) at −77.8 °C until an estimated moisture content below 5% was obtained. The preparation of BC-based nanofibers samples is shown in Fig. 1.

Fabrication of SPE membranes

BCs with a diameter of 19 mm and thickness of around 100 μm were transferred to an argon-filled glovebox with moisture level below 0.1 ppm. It was then immersed in a solution of 50 μL lithium hexafluorophosphate ($LiFP_6$) 1 M in ethylene carbonate and diethyl carbonate with the molar ratio of 1 : 1 at room temperature. Then the samples were dried at room temperature to obtain BC solvent-free or dry solid polymer electrolyte.

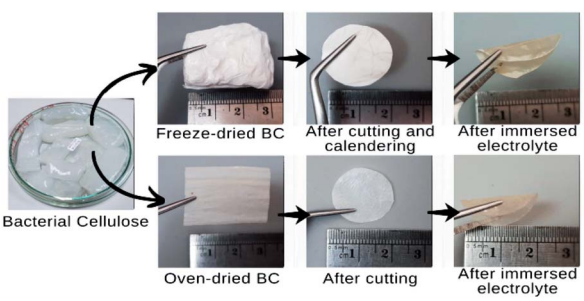

Fig. 1 Physical appearance of BC.

Structure and mechanical properties characterization

The major functional groups of BC were characterized by using FTIR spectroscopy, Thermo Fisher Scientific Nicolet iS-10. The spectra were collected using ambient air as a background over the wavelength range from 4000 to 400 cm^{-1} at room temperature. The crystallinity of the resultant materials was evaluated by using a D_2 Phase BRUKER X-ray powder diffractometer with Cu $K_{\alpha 1}$ (1.5406 Å) radiation. The tensile strength of BC membranes was tested at 25 °C with a universal testing machine, Yasuda 216-10k Universal Material Tester, which was conducted according to the ASTM D 882 method for a thin film with a tensile test speed of 5 mm min^{-1}. The length and width of the samples were 10 and 5 mm, respectively. The specimen was attached to chucks on both ends. Then, the elongation force is applied continuously through the load cell until breakage occurred. The thermal stability of the membranes was examined by using TGA PT 1600 Linseis, with a heating rate of 10 °C min^{-1} from 50° to 500° under flowing nitrogen atmosphere. The morphology of the dried BC membranes were characterized by FESEM JEOL JIB 4160F and the calculation of diameter fiber with software analysis image j. BET Surface Area and Pore Size Analyzer Quantachrome Nova 4200e is measurement based for determination of specific surface area of porous materials. The specific surface area can be estimated from the total pore volume and pore diameters. The electrolyte uptake of the membrane is the main factor for ionic conductivity.[13] The dried BC was exposed in an argon-filled glove box for 90 min to measure the electrolyte retention. The weights of BC before (W_0) and after (W_t) absorption were measured to show the liquid electrolyte uptake (η) as calculated using eqn (2)

$$\eta(\%) = \frac{W_t - W_0}{W_0} \times 100\%$$

where η is the uptake of liquid electrolyte.

Electrochemical characterization

The electrochemical stability window was characterized by linear sweep voltammetry (LSV) with a two-electrode configuration using stainless steel (SS) electrode as a working electrode and Li metal as a reference and counter electrodes. The assembly process of SS/BC-liPF_6/Li metal was conducted in a glove box filled with argon gas. LSV cyclic voltammetry (CV) and galvanostatic charge/discharge (CD) measurements were performed using WBCS3000 Automatic Battery Cycler with a constant scan rate of 5 mV s^{-1} in a potential range of 0 to 5 V at 27 °C. CR2032 coin cells were assembled using Li metal as a reference and counter electrode and $LiMnPO_4$ as a positive electrode to perform the ionic conductivity, CV, and CD measurements. Ionic conductivity properties and Li^+ transfer

© 2021 The Author(s). Published by the Royal Society of Chemistry

Open Access Article. Published on 29 June 2021. Downloaded on 12/9/2025 8:32:49 AM.
This article is licensed under a Creative Commons Attribution-NonCommercial 3.0 Unported Licence.

number of the BC membrane was measured by using EIS HIOKI 9263 SMD Test Fixture LCR with a frequency of 0.6–20 kHz.

Results and discussion

Structure and mechanical properties characterization

FTIR analysis. Fig. 2(a) shows the FTIR spectra of BCs before and after immersion in electrolyte compared with native BC gel. The main signals observed at 2919, 1636, and 1057 cm^{-1} correspond to the stretching vibration of C–H, C–C, and stretching vibration of C–O, respectively. The broad absorption peak at around 3345 cm^{-1} refers to the stretching vibration of –OH groups of water molecules, which can be clearly observed in gel BC and reduced significantly after the drying process.[14,15] The drying process of BC minimizes the accessibility of hydrogen bonds between the water molecule and hydroxyl group of cellulose structure, which can create a better affinity towards electrolyte and resist anion interference to provide smooth lithium movement.

The FTIR studies of solid polymer electrolytes focus on the carbonyl (C=O) region at 1750 cm^{-1}. In the spectra, oxygen atoms (C=O) were found on the IR spectrum of freeze-dried BC after immersion in the $LIPF_6$ electrolyte, while the IR spectrum of oven-dried BC as SPE does not show any carbonyl (C=O) region. The C=O acts as electron donors and forms a coordinate bond with Li ions from electrolyte $LiPF_6$, thereby forming polymer–salt complexes. The presence of hydroxyl groups also helps BC affinity towards electrolyte, and high electrolyte uptake builds a strong pathway for the migration of lithium ions, which enhances the ionic conductivity of the membrane electrolyte.[16]

XRD analysis. The X-ray diffractograms of oven-dried and freeze-dried BC before and after immersion in electrolyte salt are shown in Fig. 2(b). The X-ray diffractograms of commercial Celgard separator is also shown for comparison. The major diffraction peaks at 14.5°, 16.7°, and 22.6° correspond to crystalline planes of (−110), (110), and (200) for cellulose I. The crystallinity index (CI) of cellulose is calculated using the empirical method proposed by Segal *et al.*[17] as a convenient way to calculate the relative crystallinity of cellulose by using eqn (1) as follows,

$$\mathrm{CI} = 100 \times \frac{I_{200} - I_{\mathrm{am}}}{I_{200}}$$

where I_{200} is the maximum intensity of the principal peak (200) lattice diffraction, and I_{am} is the intensity of amorphous cellulose. The highest diffraction peak represents the amount of the crystalline phase, while the minimum intensity between the major peaks represents the amount of the amorphous phase.

The values of crystallinity indices of BC are 87.6% and 89.9% for freeze- and oven-dried BC, respectively. After immersion in the $LiPF_6$ electrolyte, the freeze- and oven-dried BC crystallinity index values were 86.36% and 90.43%, respectively. Freeze-dried BC before and after immersion of electrolyte solution registers a slight reduction of crystallinity than oven-dried BC. A lower degree of crystallinity value on the polymer allows the increased ionic mobility of the polymer chain as the result of a large number of Li^+ ion movements.[18,19] Celgard separator has sharp and distinct peaks around 2θ = 14.0°, 17.0°, and 18.5°, which is characteristic of isotactic polypropylene with the crystallinity degree of 31%.[20] Many researchers believe the high crystallinity could cause low ionic conductivity and low stability due to the reduced migration rate of lithium ions in the crystalline phase.[21]

Tensile analysis. Tensile test results for oven-dried and freeze-dried BC are shown in Fig. 3(b), the tensile strength is 60.17 and 14.17 MPa for freeze- and oven-dried BC, respectively, with the modulus young's is 35.8 and 7.39 MPa respectively Fig. 3(a). Mechanical strength is related to the movement of the

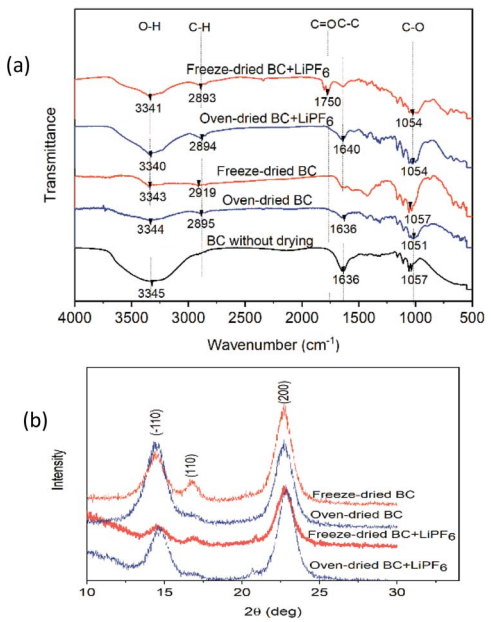

Fig. 2 (a) FTIR spectra, (b) X-ray diffractograms of freeze- and oven-dried BC membranes.

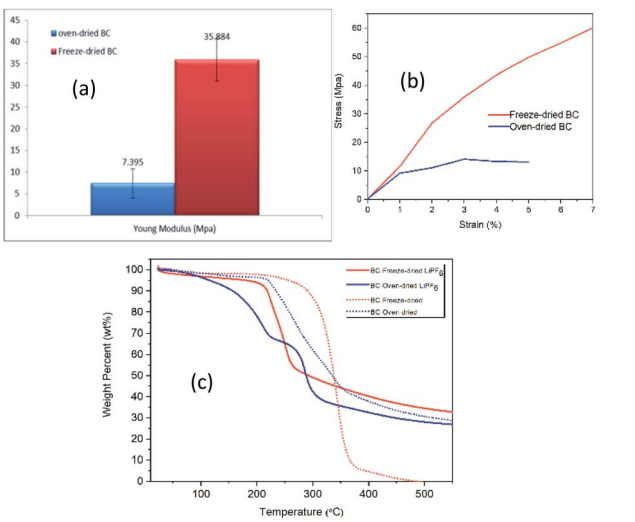

Fig. 3 (a) Young's modulus (b) Tensile stress–strain curves (c) TGA curves of freeze- and oven-dried BC membranes.

Open Access Article. Published on 29 June 2021. Downloaded on 12/9/2025 8:32:49 AM.
This article is licensed under a Creative Commons Attribution-NonCommercial 3.0 Unported Licence.

polymer chain. Low tensile strength for oven-dried BC can be linked to the network structure with higher crystallinity than freeze-dried BC.[20] The tensile property of the sample is related to the deformation resistance of the SPE membrane, which is very important in considering the rolling parameters during manufacturing.

Manufacturing procedures battery with liquid electrolyte requires separators able to sustain a stress of about 13 MPa without being damaged.[22] BC has satisfied the mechanical requirement of a separator in the LIBs system and is suitable for this application. Fan and Maier have reported the tensile study on PEO-based polymer electrolyte is 1.8 MPa, which is inferior to BC's value.

TGA analysis. Fig. 3(c) shows thermal decomposition and thermal stability of BC, before and after immersion in electrolyte salt. BC freeze dried and oven dried have different thermal stability. Drying effect causes different properties *i.e.* physical and morphological surface. Many people mention that bacterial cellulose have unique properties. They can change depending on a subjected treatment. In the beginning, freeze-dried BC show a thermal stable at 350 °C, then a drastical losses up to 370 °C and finally no observable residue was observed at 480 °C. It looks different from oven dried BC. Oven-dried BC firstly experienced weight losses at 249 °C but the sample has a smoother weight loss rate. Oven-dried BC is seem to be resisting thermal decomposition over 500 °C which is possible due to more strongly bound in the fiber network. After immersion in $LiPF_6$, two stepwise thermal decomposition was observed in oven-dried BC. More resistive thermal decomposition of $LiPF_6$ molecule inside fiber structure of oven-dried BC causes gradual decomposition (initially at 200 °C), this is in accordance with Solchenbach's statement that $LiPF_6$ dissociates completely to LiF and PF_5 at temperatures >200 °C. While presence of carbonyl (C=O) and porous structure of freezed-dried BC Fig. 4(d), makes easily thermal decomposition of $LiPF_6$. The decomposition rate depends on the temperature and the structure such as crystallinity and orientation.[23] In freeze-dried bc, there is no fiber network visible in the structure Fig. 4(c), this causes the crystallinity of freeze-dried to be lower than oven-dried. Several factors can influence thermogravimetric measurements such as pore morphology and homogeneity, which may affect heat transfer within the samples and thus influence the diffusion rate of reaction.[24,25] This result reveals that the freeze-dried BC with homogeneous porous structure can be used as a host for SPE at ambient and moderate temperatures below 250 °C, which is suitable for application in electrochemical devices, such as batteries.

Thermal stability studies of PEO polymer electrolytes exhibit minimal weight loss until the samples 200 °C; this indicates that the PEO–$LiPF_6$ is stable up to 200 °C before decomposition. At 200 °C, the $LiPF_6$ starts to melt, and the system is no longer stable.[26] SPE, which is assembled in a lithium-ion battery system, is generally operated at a temperature higher than room temperature, typically cycled at 50–80 °C to achieve good performance.[27] Thermal stability is vital for solid polymer electrolytes in Li-ion battery applications.[28] PP separator shows large thermal shrinkage; the weight loss was seen at around 50–100 °C is attributed to the decomposition.[29] Resultantly, compared to the commercial PP separator and PEO polymer electrolytes, the BC membrane presents higher thermal stability.

Morphology of BC as SPE. Fig. 4(a) shows the FESEM images of oven-dried BCs. The surface view shows many interrelated strings and very short inter-fiber distance of cellulose structure. It is predominated by hydrogen bond interaction, suggests the permanent closure of pores structure. High concentration of hydrogen bonding present in the BC oven-dried surface, creating clusters with a strong attraction of BC interlayer, which hinders the individual separation of these cellulose crystal structures. Freeze drier technique is drying process of water from cellulose fiber network through the process of sublimation and the removal of bound water molecules through the process of desorption without shrinkage present in freeze-dried fiber Fig. 4(c), which causes a larger inter-fiber distance to form three dimensional pore structures. Three-dimensional pore structures provide plenty of Li-ion sites for ionic mobility. Fig. 4(b) and (d) shows the morphological surface of oven-dried and freeze-dried BC as SPE after immersed in $LiPF_6$. The figures display a detailed structure of homogeneous and interweave nanofibrous randomly to build up a porous and cross-linking structure. The image of oven-dried BC shows a relatively dense and less pore structure. Oven-dried has an impact on a greater surface tension force, which pulls the pores into smaller ones. The image of freeze-dried BC shows a relatively smooth and compact pore surface. Pores among active materials generate electrolyte molecules diffusion through the cellulose structure to promote ion transport. The cross-linking network structure of freeze-dried BC ensures the superior mechanical strength of BC, providing an excellent absorption of the electrolyte. The flexibility of BC as SPE is highly correlated with the 3D interconnected nanofibrous network and the conformal structure. The porous structures of the presented membranes allowed a significant amount of liquid electrolyte to be absorbed in matrix.[30] Based on morphological pore analysis using Image J, Fig. 5(a) and (c) shown distribution histograms

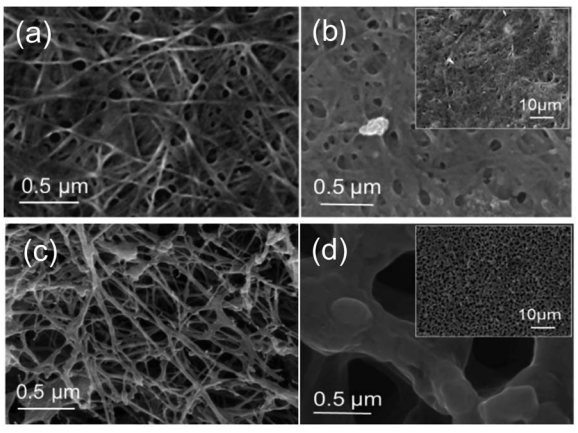

Fig. 4 Morphology of (a) oven-dried BC, (b) oven-dried BC after immersed in $LiPF_6$, (c) freeze-dried BC, and (d) freeze-dried BC after immersed in $LiPF_6$.

© 2021 The Author(s). Published by the Royal Society of Chemistry

Open Access Article. Published on 29 June 2021. Downloaded on 12/9/2025 8:32:49 AM.
This article is licensed under a Creative Commons Attribution-NonCommercial 3.0 Unported Licence.

diameter fiber of oven-dried and freeze-dried BC are 24.8 nm and 21.3 nm, respectively. Meanwhile Fig. 5(b) and (d) explain of distribution histograms diameter BC freeze-dried after immersed $LiPF_6$ electrolyte expanded highly about 270.7 nm than those oven-dried BC 48.4 nm. It is relevant on electrolyte uptake properties oven-dried and freeze-dried BC about 99,4% and 167,7% respectively. The elements of oven-dried and freeze-dried BC as SPE after the charge–discharge process is examined by energy-dispersive X-ray spectroscopy (EDS), as shown in Fig. 5(e) and (f). The EDS investigation indicate of elemental distribution, which freeze-dried BC shows the higher content of P and F atoms than oven-dried BC representing $LiPF_6$ electrolyte absorption in the sample.

Surface area analysis. Table 1 shows the N_2 adsorption–desorption analysis. The measurement is based on physical adsorption of gas on the sample surface. The amount of gas can be defined by the Langmuir isotherm assuming a monolayer of gas molecules on the homogenous surface which are not mutually affected. The determined values of specific surface area are dependent on the used adsorbing gas—lower values are obtained with larger molecules. Usually nitrogen or argon is used. The data in the table shows freeze-dried BC has a surface area of 439 $m^2\ g^{-1}$, more extensive than that of oven-dried BC, which is 122 $m^2\ g^{-1}$. The large surface area is almost close to the commercial surface area of Celgard separator 463 $m^2\ g^{-1}$ with thickness 40 μm and pore volume 0.529.[31] The surface area possesses unique intrinsic properties, such as abundant functional moieties and uniform dispersibility, showing remarkable mechanical strength.[32] The number of pores in each unit area of the sample is affected by the pore size, pore shape, and pore composition in BC samples. The large specific surface area enables better interfacial interactions between Li-ion and the polymer matrix if pore structures are uniformly dispersed throughout the matrix. Hierarchical micropore – the mesoporous structure and high surface area contribute to improving lithium storage performance. Pore volume can contain large amounts of Li^+.[33] Surface of BC has a hydroxyl group, which is liable to form hydrogen bonds with PF_6^- and other anions. The interactions hinder the movement of anions in the electrolyte and increase the number of transferred lithium ions and high specific surface area, which are desired during the charge–discharge.

Table 1 BET measurement

Sample	Surface area ($m^2\ g^{-1}$)	Pore volume ($cm^3\ g^{-1}$)	Thickness (μm)
BC oven-dried	122	0.685	80
BC freeze-dried	439	0.535	34

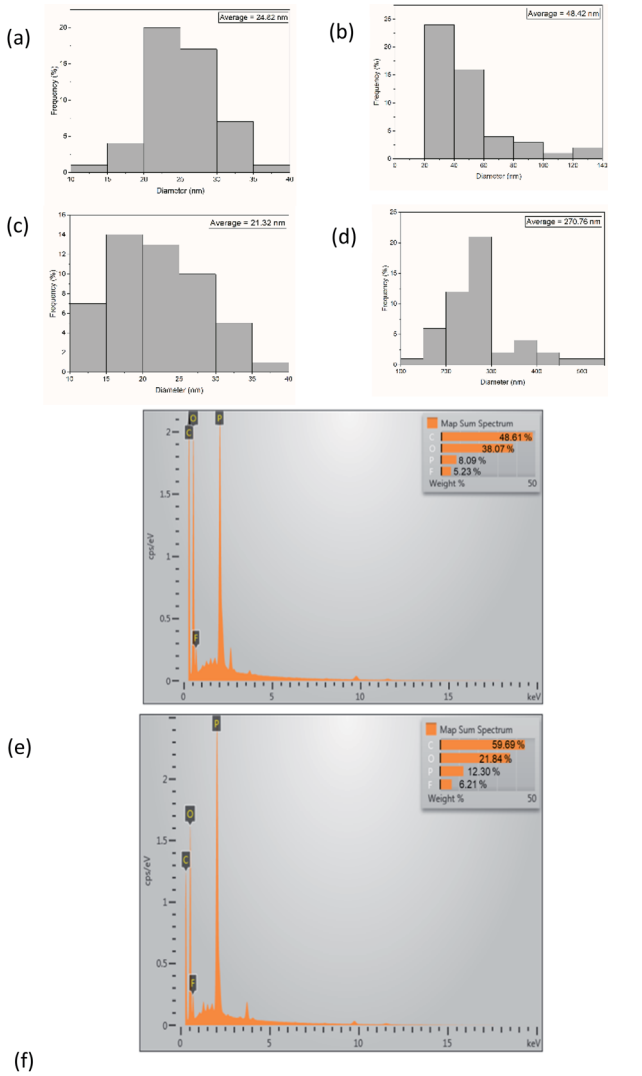

Fig. 5 Fiber diameter distribution histograms of oven-dried BC, (b) oven-dried BC after immersed in $LiPF_6$, (c) freeze-dried BC, (d) freeze-dried BC after immersed in $LiPF_6$ and elemental analysis of BC after the charge–discharge process (e) oven-dried, (f) freeze-dried.

Electrochemical characterization

EIS measurement. Fig. 6(a) shows charge-transfer resistances by the semicircle Nyquist plot of all samples. The Nyquist plot compares the real component rather than the impedance over a specific frequency range. This analysis describes phenomena related to the rate of electrochemical reactions in the battery cell. The electrochemical reaction between the electrolyte and electrode is indicated by the depressed region of semicircles in the mid to high-frequency range, which represents charge transfer resistance (R_{ct}) inside the battery cell.[34] Ionic conductivity can be calculated by using eqn (3);

$$\tau = \frac{I}{A \times R_s}$$

where τ, l, A, and R_s represent ionic conductivity, SPE thickness, SPE-electrode contact area, and SPE resistance, respectively. The ionic conductivity is shown in Table 2. The ionic conductivity value of freeze-dried BC is higher than that of oven-dried BC, which is 2.71×10^{-2} S cm^{-1}. This value is better than the ionic conductivity of biopolymer membranes. The ionic conductivity of biopolymeric SPEs at room temperature such as lignin (10^{-7} to 10^{-5} S cm^{-1}), chitosan (0.066×10^{-3} S cm^{-1}) and

Open Access Article. Published on 29 June 2021. Downloaded on 12/9/2025 8:32:49 AM.
This article is licensed under a Creative Commons Attribution-NonCommercial 3.0 Unported Licence.

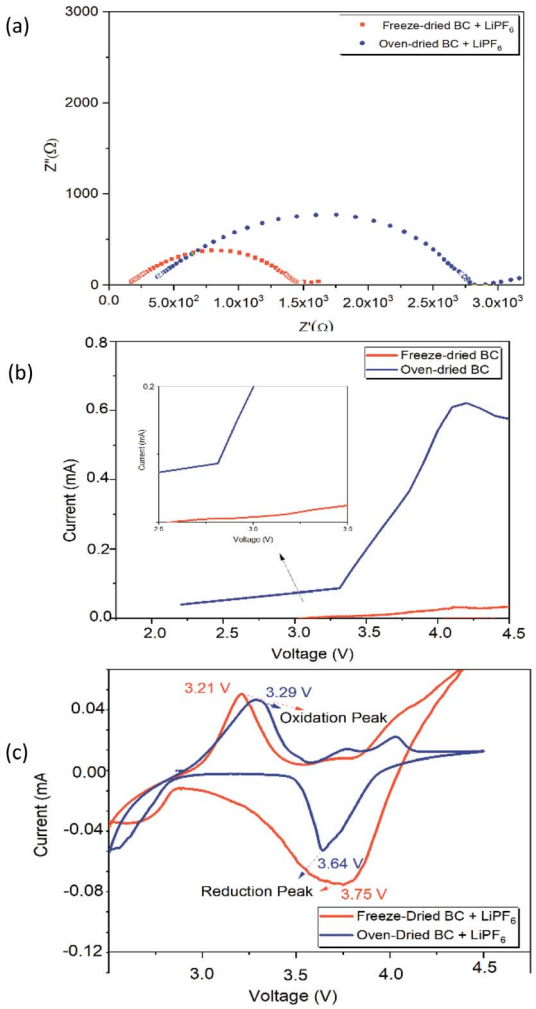

Fig. 6 (a) Nyquist plot of freeze- and oven-dried BC obtained from EIS measurement. (b) LSV of freeze- and oven-dried BC as SPE (c) CV of the freeze-and oven- BC as SPE.

Table 2 Ionic conductivity measurement

Sample	Ionic conductivity (S cm^{-1})
BC freeze dry + $LIPF_6$	2.71×10^{-2}
BC oven dry + $LIPF_6$	6.00×10^{-3}

algae (1.15×10^{-3} S cm^{-1}).[35] Despite this, the presence of a large number of polar groups in biopolymer help dissolves a significant concentration of salts *via* Lewis acid–base interactions and electrostatic forces, which is necessary for achieving a significant ionic conductivity.[35] The ionic conductivity is thus not only directly linked to the polymer dynamics, where high conductivity is possible under the low-temperature drying condition of the BC freeze-dried polymer. The higher freeze-dried BC conductivity value is obtained due to higher amounts of hydrogen bonds with anions of lithium salts, to promote the dissociation of lithium salts and facilitate the migration of lithium ions. We take Li/BC $LiPF_6$/Li to measure Li^+ transfer number. Freeze dried bc have better value Li^+ transfer number than oven dried bc which is 0.48 and 0.2. The polar functional hydroxyl on the freeze-dried BC can not only enhance the salt dissociation beneficial to lithium ionic conductivity but also be used as a trapper for the anion of most lithium salt mostly owing to the hydrogen bond between them. The ionic conductivity of a polymer electrolyte is influenced by the mobility and concentration of the conducting species (cation and anion).[36] Lower crystallinity index promotes the transportation of ions on freeze-dried BC and increases the ionic conductivity.[37] These properties appear to be better demonstrated by the BC prepared by the freeze-drying.

Linear sweep voltammetry (LSV). The voltammogram on the electrochemical stability window of BC containing $LiPF_6$ electrolyte is plotted in Fig. 6(b). The onset of the oven-dried BC plot shows observed current flow sharply increases at 2.2 V. Electrochemical stability window of freeze-dried BC is almost constant. The current is steady-state at a low current of 0.02 mA from 2.0 to 3.5 V, which indicates the electrolyte is electrochemically stable in this voltage range. During the positive scan, a small broad peak at 4.0 V is observed, which could be correlated to film formation with passivating behavior at the working electrode side. Above this value, the sharp current increase is due to the decomposition of the electrolyte. This result shows that freeze-dried BC is electrochemically stable up to 3.5 V and is suitable to be applied in a lithium-based battery below 4 V. The electrochemical stability window or anodic stability of freeze-dried BC is higher than that of oven-dried BC, which is similar to that of the commercialized Celgard membrane soaked with liquid electrolyte.[38]

The electrochemical stability (*i.e.*, working cell potential range) of SPE is an essential criterion for its application of electrochemical devices.[2] In linear sweep voltammetry (LSV), a potential which varies linearly with time is applied between an initial potential and a final potential (LSV) or cycled between two extreme (or switching) potential values at a given potential scan rate ν (usually expressed in mV s^{-1}). The optimum electrochemical stability window of BC is an essential requirement for choosing suitable electrolytes for the application of Li-ion batteries.

Cyclic voltammetry (CV). The test results of BC as SPE assembled in half-cell lithium batteries are presented on CV curves in Fig. 6(c). CV was carried out to examine whether the reversible reduction–oxidation reaction occurs. Oxidation/reduction peaks at about 3.20/3.75 V correspond to freeze-dried BC as SPE, 3.29/3.64 V for oven-dried BC as SPE, which corresponds to the cyclic voltammetry oxidation/reduction peaks and consistent with $LiMnPO_4$ cathode tested in a liquid electrolyte with Celgard separator. Oxidation/reduction peaks suggest that the reaction current is derived from both diffusion-controlled Li^+ intercalation–deintercalation.[39] CV is a technique which is conducted by applying a voltage that changes linearly on an electrode. CV provides information about the characteristic of redox reaction in electrode, which can be attributed to the electrode porosity of active materials and the internal resistance, thus creating a current dependence of voltage.[40]

© 2021 The Author(s). Published by the Royal Society of Chemistry

Open Access Article. Published on 29 June 2021. Downloaded on 12/9/2025 8:32:49 AM.
This article is licensed under a Creative Commons Attribution-NonCommercial 3.0 Unported Licence.

Galvanostatic charge–discharge (CD). CD measurement was conducted to examine the maximum capacity through voltage exposure. The CD profiles of BC as SPEs are shown in Fig. 7(a) and (b). Freeze-dried BC has a higher charging voltage than oven-dried BC. It means that oven-dried BC consumes less energy at the charging condition. The specific discharge capacities of freeze and oven-dried BC are 18 mA h g^{-1} at 0.2C and 5.6 mA h g^{-1} at 0.5C (Fig. 7(a)), and 0.3 mA h g^{-1} at 0.2C and 0.075 mA h g^{-1} at 0.5C (Fig. 7(b)), respectively. Therefore, the discharge capacity of $LiFePO_4$ tested with BC polymer electrolyte is still far from that tested traditional liquid electrolyte; Celgard separator has the highest specific capacity value of 92.9 mA h g^{-1} at 0.2C and 45.8 mA h g^{-1} at 0.5C. The BC membrane's electrochemical performance was evaluated by fabricating a battery using $LiMnPO_4$ as the cathode material and BC as the electrolyte and separator.

During the charge–discharge cycling process of Li-ion batteries, anions such as PF_6 in the electrolyte are also movable besides lithium-ion transfer. Those anions will probably concentrate and be absorbed or decomposed on the surface of electrodes during the cycles, thus will affect the performance of the battery. The significant capacity decrease may be attributed to the degradation of the electrolytes.[41] These different performances are given because, during the discharge, the low porosity of the oven-dried BC as SPE acts as a bridge for the migration of ions, limiting their diffusion towards the positive electrode. The better specific capacity of freeze-dried BC as SPE is related to the ionic conductivity of SPE.[42] When freeze-dried BC is in contact with the electrode, its porous structure allows a quick diffusion during the discharge process, which effectively improves lithium ions' mass transport. The concentration polarization resistance increases and consumes Li^+, caused by partly irreversible electrode reaction and thickened solid-electrolyte interphase film during the cycle process.[43]

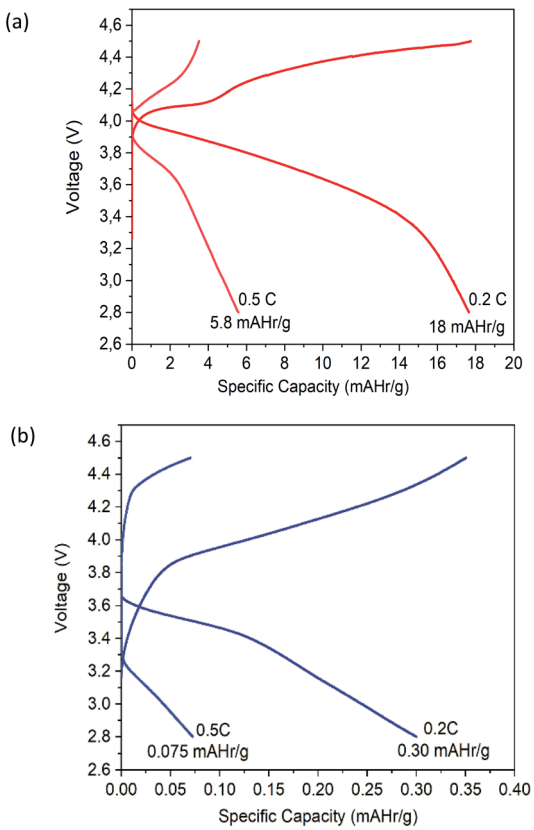

Fig. 7 (a) CD of freeze-dried NFC, (b) CD of oven-dried NFC.

Conclusions

This study showed that different drying methods affect the structure, mechanical properties, and electrochemical performance of BC as SPE. Freeze-dried BC showed significant interactions between Li^+ ions from the salt and the C=O groups. It has a crystallinity index of 86.36%, an excellent tensile strength of 60.17 MPa, the thermal stability of up to 250 °C, and a homogeneous porous structure with a high surface area. This BC was achieved by the frozen substance when sublimation occurred. The electrochemical performances of freeze-dried BC as SPE is better than those of oven-dried BC, such as higher ionic conductivity of 2.71 × 10^{-2} S cm^{-1}, higher stability window beyond 3.5 V, oxidation/reduction peaks of 3.29/3.64 V, and specific capacity of 18 mA h g^{-1} at 0.2C and 5.6 mA h g^{-1} at 0.5C. The structure and morphology of freeze-dried BC still need to be optimized to get SPE with better electrochemical performance. Despite the current results, the freeze-dried BC can be applied as SPE in lithium-ion batteries since BC is environmentally friendly and can be produced by using a low-cost method.

Conflicts of interest

There are no conflicts to declare.

Acknowledgements

The authors would like to gratefully acknowledge all kind of supports from the Japan Society for The Promotion of Science in the form of the RONPAKU Program, Department of Applied Chemistry, Graduate School of Engineering Osaka University, Research Center for Physics – Indonesian Institute of Sciences and its Advanced Characterization Laboratories Serpong through E-Layanan Sains for the facilities, scientific, and technical support. Financial support for this publication was provided by RISPRO PRN "Litbang Pembesaran Skala Produksi Bahan Baku Baterai Lithium Merah Putih 83/E1/PRN/2020". The authors would also thank Dr Rizna Triana Dewi and Mr Muhammad Ghozali for the immense help on the sample preparations of freeze-dried and tensile strength measurement.

References

1 P. Barai, K. Higa and V. Srinivasan, *Phys. Chem. Chem. Phys.*, 2017, **19**, 20493–20505.
2 L. Long, S. Wang, M. Xiao and Y. Meng, *J. Mater. Chem. A*, 2016, **4**, 10038–10039.

Open Access Article. Published on 29 June 2021. Downloaded on 12/9/2025 8:32:49 AM.
This article is licensed under a Creative Commons Attribution-NonCommercial 3.0 Unported Licence.

3 Z. Gadjourova, Y. G. Andreev, D. P. Tunstall and P. G. Bruce, *Nature*, 2001, **412**, 520–523.
4 B. S. Kumar Jr and G. Lawrence, *US pat.*, 6190806, USPTO, 2000.
5 S. Cho, S. Kim, W. Kim, S. Kim and S. Ahn, *Polymers*, 2018, **10**, 1–16.
6 Z. Wang, H. Gu, Z. Wei, J. Wang, X. Yao and S. Chen, *Ionics*, 2019, **25**, 907–916.
7 Y. S. Wu, C. C. Yang, S. P. Luo, Y. L. Chen, C. N. Wei and S. J. Lue, *Int. J. Hydrogen Energy*, 2017, **42**, 6862–6875.
8 D. Lasrado, S. Ahankari and K. Kar, *J. Appl. Polym. Sci.*, 2020, **137**, 1–14.
9 K. Y. Chua, A. D. Azzahari, C. N. Abouloula, F. Sonsudin, N. Shahabudin and R. Yahya, *J. Polym. Res.*, 2020, **27**(5), 115.
10 R. Pan, Z. Wang, R. Sun, J. Lindh, K. Edström, M. Strømme and L. Nyholm, *Cellulose*, 2017, **24**, 2903–2911.
11 C. Campano, A. Balea, A. Blanco and C. Negro, *Cellulose*, 2016, **23**, 57–91.
12 Y. Hu and J. M. Catchmark, *Am. Soc. Agric. Biol. Eng. Annu. Int. Meet.*, 2009, **8**, 5274–5288.
13 G. Yang, H. Cai, X. Li, M. Wu, X. Yin, H. Zhang and H. Tang, *RSC Adv.*, 2020, **10**, 5077–5087.
14 L. Indrarti, Indriyati, A. Syampurwadi and S. Pujiastuti, *AIP Conf. Proc.*, 2016, **1711**, DOI: 10.1063/1.4941633.
15 R. Yudianti, A. Syampurwadi, H. Onggo, M. Karina, H. Uyama and J. Azuma, *Polym. Adv. Technol.*, 2016, **27**, 1102–1107.
16 M. R. Asghar, M. T. Anwar, A. Naveed and J. Zhang, *Membranes*, 2019, DOI: 10.3390/membranes9070078.
17 L. Segal, J. J. Creely, A. E. Martin and C. M. Conrad, *Text. Res. J.*, 1959, **29**, 786–794.
18 D. Zhao, Y. Zhu, W. Cheng, W. Chen, Y. Wu and H. Yu, *Adv. Mater.*, 2020, **2000619**, 1–18.
19 S. Jafirin, I. Ahmad and A. Ahmad, *BioResources*, 2013, **8**, 5947–5964.
20 C. T. Love, *J. Power Sources*, 2011, **196**, 2905–2912.
21 J. A. Matthews, *Encycl. Environ. Chang.*, 2014, DOI: 10.4135/9781446247501.n1321.
22 Q. Fu, G. Lin, X. Chen, Z. Yu, R. Yang, M. Li, X. Zeng and J. Chen, *Energy Technol.*, 2018, **6**, 144–152.
23 Z. Cai and J. Kim, *Cellulose*, 2010, **17**, 83–91.
24 B. Ravdel, K. M. Abraham, R. Gitzendanner, J. DiCarlo, B. Lucht and C. Campion, *J. Power Sources*, 2003, **119–121**, 805–810.
25 D. Kotatha, K. Morishima, S. Uchida, M. Ogino, M. Ishikawa, T. Furuike and H. Tamura, *Res. Chem. Intermed.*, 2018, **44**, 4971–4987.
26 S. Ibrahim and M. R. Johan, *Int. J. Electrochem. Sci.*, 2012, **7**, 2596–2615.
27 S. T. Hsu, B. T. Tran, R. Subramani, H. T. T. Nguyen, A. Rajamani, M. Y. Lee, S. S. Hou, Y. L. Lee and H. Teng, *J. Power Sources*, 2020, **449**, 227518.
28 M. Li, X. Wang, Y. Wang, B. Chen, Y. Wu and R. Holze, *RSC Adv.*, 2015, **5**, 52382–52387.
29 M. Raja and A. M. Stephan, *RSC Adv.*, 2014, **4**, 58546–58552.
30 N. Li, J. Zheng, P. Hadi, M. Yang, X. Huang, H. Ma, H. W. Walke and B. S. Hsiao, *Membranes*, 2019, **9**(6), DOI: 10.3390/membranes9060070.
31 J. Weidner, *ECS Trans.*, 2009, **19**, 30.
32 H. Ben Youcef, B. Orayech, J. M. L. Del Amo, F. Bonilla, D. Shanmukaraj and M. Armand, *Solid State Ionics*, 2020, **345**, 115168.
33 Y. Xia, W. S. Xiong, Y. Jiang, W. Sun, H. Q. Sang, R. X. He, Q. Tai, B. Chen, Y. Liu and X. Z. Zhao, *RSC Adv.*, 2017, **7**, 21988–21996.
34 H. Raj, S. Singh and A. Sil, *Electrochim. Acta*, 2019, **326**, DOI: 10.1016/j.electacta.2019.134981.
35 E. Lizundia and D. Kundu, *Adv. Funct. Mater.*, 2021, **31**, 1–29.
36 T. K. Lee, N. F. M. Zaini, N. N. Mobarak, N. H. Hassan, S. A. M. Noor, S. Mamat, K. S. Loh, K. H. KuBulat, M. S. Su'ait and A. Ahmad, *Electrochim. Acta*, 2019, **316**, 283–291.
37 M. Rayung, M. M. Aung, S. C. Azhar, L. C. Abdullah, M. S. Su'ait, A. Ahmad and S. N. A. M. Jamil, *Materials*, 2020, **13**(4), DOI: 10.3390/ma13040838.
38 L. Singheiser, P. Huczkowski, T. Markus and W. J. Quadakkers, *Shreir's Corrosion*, 2010, pp. 482–517.
39 A. Arya and A. L. Sharma, Polymer electrolytes for lithium ion batteries: a critical study, *Ionics*, 2017, **23**(3), 497–540.
40 N. M. J. Rasali, M. A. Saadiah, N. K. Zainuddin, Y. Nagao and A. S. Samsudin, *Express Polym. Lett.*, 2020, **14**, 619–637.
41 S. B. Aziz, T. J. Woo, M. F. Z. Kadir and H. M. Ahmed, *J. Sci. Adv. Mater. Devices*, 2018, **3**, 1–17.
42 C. M. Costa, Y. H. Lee, J. H. Kim, S. Y. Lee and S. Lanceros-Méndez, *Energy Storage Mater.*, 2019, **22**, 346–375.
43 Y. Liu, J. Chen, Z. Liu, H. Xu, Y. Zheng, J. Zhong, Q. Yang, H. Tian, Z. Shi, J. Yao and C. Xiong, *J. Alloys Compd.*, 2020, **829**, 154541.

© 2021 The Author(s). Published by the Royal Society of Chemistry